# Electronic Supplementary Information

## High Iodine Uptake in Two-Dimensional Covalent Organic Frameworks

Lingyan Zhang,[ac] Jinheng Li,[ac] Huixin Zhang,[a] Yu Liu,[ab] Yumeng Cui,[a] Fenchun Jin,[a] Ke Wang,[a] Guiyan Liu,*[a] Yanli Zhao*[b] and Yongfei Zeng*[a]

[a]Tianjin Key Laboratory of Structure and Performance for Functional Molecules, Key Laboratory of Inorganic-Organic Hybrid Functional Material Chemistry (Ministry of Education), College of Chemistry, Tianjin Normal University, Tianjin, 300387 (P. R. China). E-mail: guiyanliu2013@163.com; yfzeng@nankai.edu.cn.

[b]Division of Chemistry and Biological Chemistry, School of Physical and Mathematical Sciences, Nanyang Technological University, 21 Nanyang Link, 637371 Singapore (Singapore). E-mail: zhaoyanli@ntu.edu.sg.

[c]These authors contributed equally to this work.

## Section S1: Experimental Section

**Materials.** 1,3,5-Trimethyl-2,4,6-tris(4-aminophenyl)benzene was synthesized according to literature methods.[S1] Terephthalaldehyde was purchased from Shanghai Dibo Biotechnology Co., Ltd. 2,5-Dihydroxy-1,4-benzenedicarboxaldehyde was purchased from Jilin Yanshen Technology Co., Ltd (Changchun, China). Iodine was purchased from Kmart (Tianjin) Chemical Technology Co., Ltd. N,N-Dimethylformamide (99.5%) and tetrahydrofuran (99.0%) were purchased from Tianjin JingDongTianZheng Precision Chemical Reagent Factory (Tianjin, China). *n*-Butanol (99%) and 1,2-dichlorobenzene (99%) and were purchased from Sigma Aldrich Chemicals.

**Analytical techniques.** Powder X-ray diffraction (PXRD) measurements were performed on a 40 kV, 40 mA Bruker D8 Advance diffractometer using Cu-Kα radiation over 2θ range of 3º-30º at room temperature. Fourier transform infrared (FT-IR) spectra of samples prepared as KBr pellets were recorded on a Nicolet IR200 FT-IR spectrometer. The solid-state $^{13}C$ NMR spectra of COFs were recorded on a VARIAN Infinity plus 300 MHz. Thermogravimetric analysis (TGA) was performed on a TGA Q500 thermoanalyzer with a nitrogen flow of 60 mL/min at a heating rate of 15 ºC/min. Scanning electron microscope (SEM) images were measured by the FEI Nova Nano 230 Field-Emission device with 15 kV acceleration voltages, and all the samples were sputtered with metallic gold (2×90 s). Gas sorption analyses were conducted using Quantachrome Instruments Autosorb-iQ-MP-MP with extra-high pure $N_2$. The Brunauer-Emmett-Teller (BET) surface area and pore size distribution were calculated based on the $N_2$ adsorption/desorption isotherm at 77 K. The calculation of BET surface area was performed using the software provided in Quantachrome. The selection of the isothermal points used to calculate the BET surface area follows three consistent criteria. First, the pressure range selected should have values of $v(P_0-P)$ increasing with $P/P_0$. Second, the points used to calculate the BET surface area must be linear with an upward slope. Third, the line they form must have a positive y-intercept. The pore size distribution was calculated based on the Quenched-Solid Density Functional Theory (QSDFT equilibrium model on carbon containing slit/cylindrical pores) model in the Quantachrome ASiQwin 3.01 software package. UV/visible (UV/vis) spectra of the solutions were recorded using a UV-2600 UV/vis spectrophotometer within the wavelength range of 200-600 nm. The Raman spectra were recorded on a Thermo Fisher DXR equipped with a 532 nm laser. All the COF samples treated by THF were loaded into a sample cell and dried under vacuum at 60 °C and 150 °C by using the “outgasser” function for 1 h and

12 h before the measurements, respectively. X-ray photoelectron spectroscopy (XPS) was performed using Thermo ESCALAB 250XI X-ray photoelectron spectrometer. Calibration charts for UV/vis spectra of standard iodine in methanol solution, as well as the fitting charts for absorbance values and iodine concentrations are based on the reference report.[S1]

**Synthesis of TJNU-203 (or TJNU-204)**. TMTAPB (19.6 mg, 0.05 mmol) and TPA (10.1 mg, 0.075 mmol) (or DHA (12.5 mg, 0.075 mmol)) were added to a 10 mL Schlenk tube. Then, 1,2-dichlorobenzene (0.5 mL), n-butanol (0.5 mL) and aqueous acetic acid (0.2 mL, 3M) were added to the above mixture. After sonication for 15 minutes, the tube was rapidly frozen under a 77 K liquid nitrogen bath, evacuated and screwed up. The tube was placed in an oven and heated at 120 °C for 3 days. After cooling down to the room temperature, a yellow (or orange-red) precipitate was obtained by filtration, followed by washing with N,N-dimethylformamide and tetrahydrofuran (THF). Pure TJNU-203 (or TJNU-204) was obtained by extracting with THF for 12 hours and drying under vacuum.

**General procedure**. The iodine vapor uptake and release, as well as the recycling experiments were carried out for three parallel tests, and the final data were shown on average.

**Iodine vapor capture**. Activated TJNU-203 (or TJNU-204) sample (20 mg) was placed in a vial (5 mL), which was then exposed in a sealed container (20 mL) containing iodine (800 mg). Next, the sealed container (20 mL) was heated at 77 °C for different hours. After cooling down to room temperature, the vial with the $I_2$@TJNU-203 (or $I_2$@TJNU-204) sample was taken out, and treated under vacuum for 1 hour to remove surface-adsorbed iodine. The $I_2$@TJNU-203 (or $I_2$@TJNU-204) sample was collected and then weighed. For recycling experiments, the $I_2$@TJNU-203 (or $I_2$@TJNU-204) sample was heated at 125 °C for 24 hours, and used for the next adsorption experiment after cooling down to room temperature.

In order to verify the adsorption occurring within the 1D channels rather than the surface condensation, the retention experiments of $I_2$-loaded samples were carried out at room temperature and ambient pressure. $I_2$@TJNU-203 and $I_2$@TJNU-204 samples containing 5.885 g/g and 5.335 g/g iodine were placed at room temperature under ambient pressure for five days, respectively. Five days later, $I_2$@TJNU-203 and $I_2$@TJNU-204 were weighed. The experiment was carried out three times in parallel and the calculation results were the average values of three times. The adsorption capacity of iodine was 5.505 g/g for $I_2$@TJNU-203 and 4.98 g/g

for $I_2$@TJNU-204. The results indicate that there is no significant iodine loss, indicating that the adsorption occurs within the 1D channels rather than the surface condensation.

**Iodine release**. The process of releasing iodine from $I_2$@TJNU-203 (or $I_2$@TJNU-204) was performed in methanol at room temperature, and the process was monitored by UV/visible spectroscopy. $I_2$@TJNU-203 (or $I_2$@TJNU-204) (10 mg) was added to methanol (300 mL) and stirred at room temperature. A solution (3 mL) was transferred out at different times and then filtered through 0.45 μm polytetrafluoroethylene membrane to remove any trace residual particulates, which was then measured by UV/visible spectroscopy.

**Calculation methods.** Grand canonical Monte Carlo simulations were used to calculate $I_2$ adsorption (Figures S30 and S31). In the grand canonical ensemble, the chemical potential of each component, the temperature and the volume were fixed. Numbers of molecules were then allowed to fluctuate until the required chemical potential was attained. The Lennard-Jones parameters for the structures were taken from the compass force field and the coulombic interactions were calculated using Ewald summation technique.[S2-S4] The structure and accurate adsorptive configuration of the COFs were optimized by Density functional theory (DFT) calculations. When carried out the DFT calculations, Perdew-Burke-Ernzerhof (PBE) exchange-correlation functional was used with a plane wave pseudopotential implementation. The kinetic energy cutoff was set to 380 eV. The model was a periodic unit cell (1×1×1). All atoms were completely relaxed to obtain accurate structures. The adsorptive enthalpy was calculated according to $\Delta E = \Delta E_0 - \Delta ZPE$, where $\Delta E_0$ is the energy change of each state calculated at 0 K, and $\Delta ZPE$ is the variation in zero point energy (ZPE).

## Section S2: Fourier Transform Infrared (FT-IR) Spectroscopy

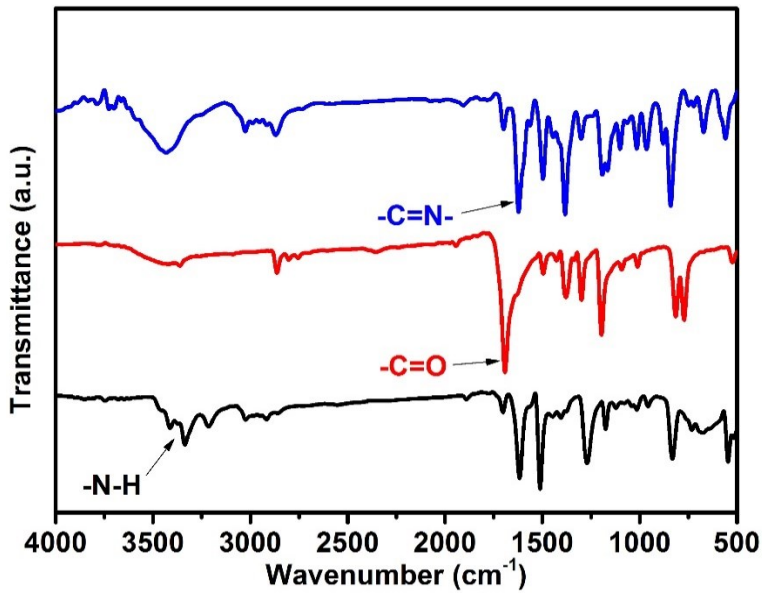


**Figure S1.** FT-IR spectra of 1,3,5-trimethyl-2,4,6-tris(4-aminophenyl)benzene (black line), terephthalaldehyde (red line) and TJNU-203 (blue line).

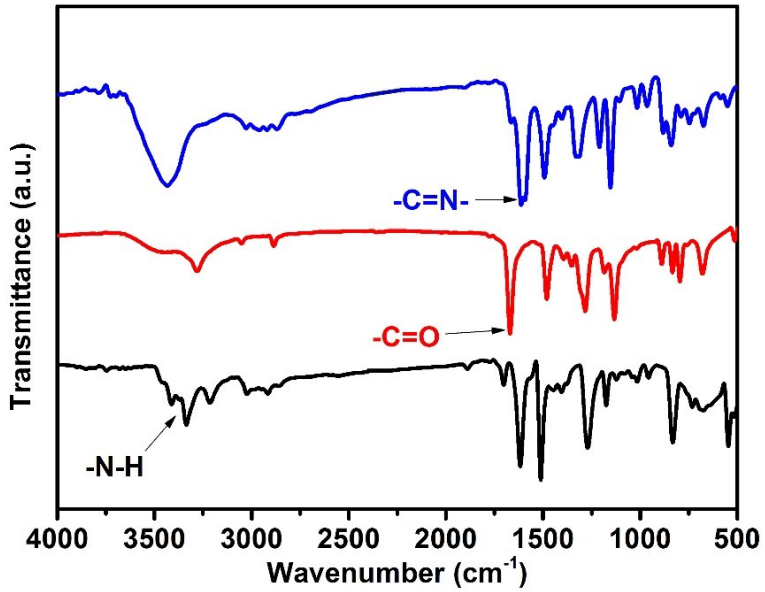


**Figure S2.** FT-IR spectra of 1,3,5-trimethyl-2,4,6-tris(4-aminophenyl)benzene (black line), 2,5-dihydroxy-1,4-benzenedicarboxaldehyde (red line) and TJNU-204 (blue line).

## Section S3: Nuclear Magnetic Resonance (NMR) Spectroscopy

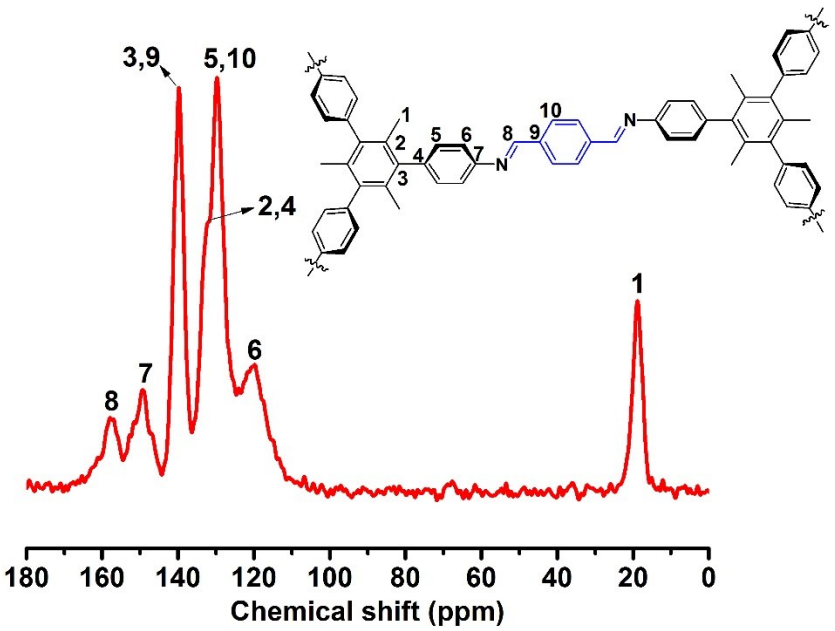


| Carbon number | Chemical shift (ppm) |
|---|---|
| 1 | 18 |
| 2 | 132 |
| 3 | 139 |
| 4 | 132 |
| 5 | 129 |
| 6 | 119 |
| 7 | 149 |
| 8 | 157 |
| 9 | 139 |
| 10 | 129 |

**Figure S3.** Solid-state $^{13}C$ NMR spectra and peak assignments of TJNU-203.

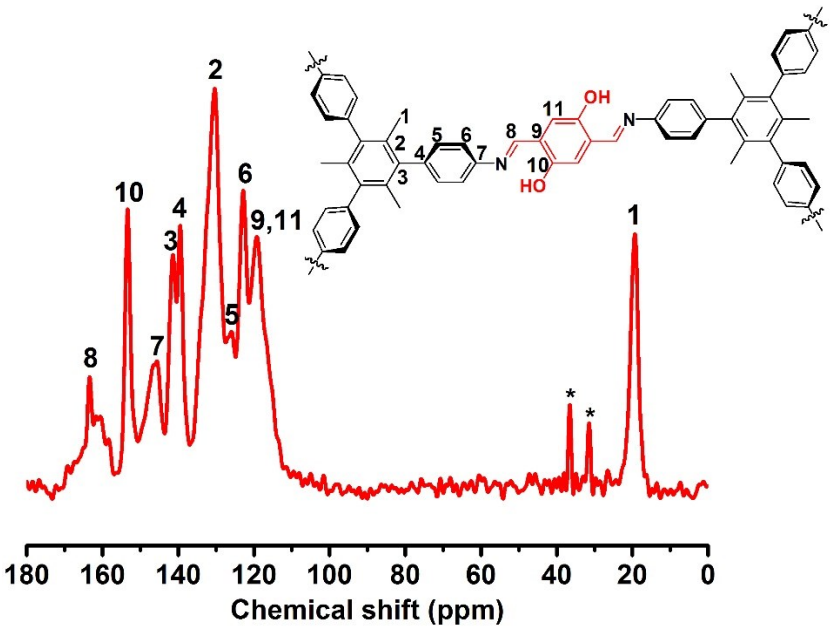


| Carbon number | Chemical shift (ppm) |
|---|---|
| 1 | 19 |
| 2 | 130 |
| 3 | 141 |
| 4 | 139 |
| 5 | 126 |
| 6 | 122 |
| 7 | 145 |
| 8 | 163 |
| 9 | 119 |
| 10 | 153 |
| 11 | 119 |

**Figure S4.** Solid-state $^{13}C$ NMR spectra and peak assignments of TJNU-204. Asterisks denote spinning sidebands.

## Section S4: Scanning Electron Microscope (SEM)

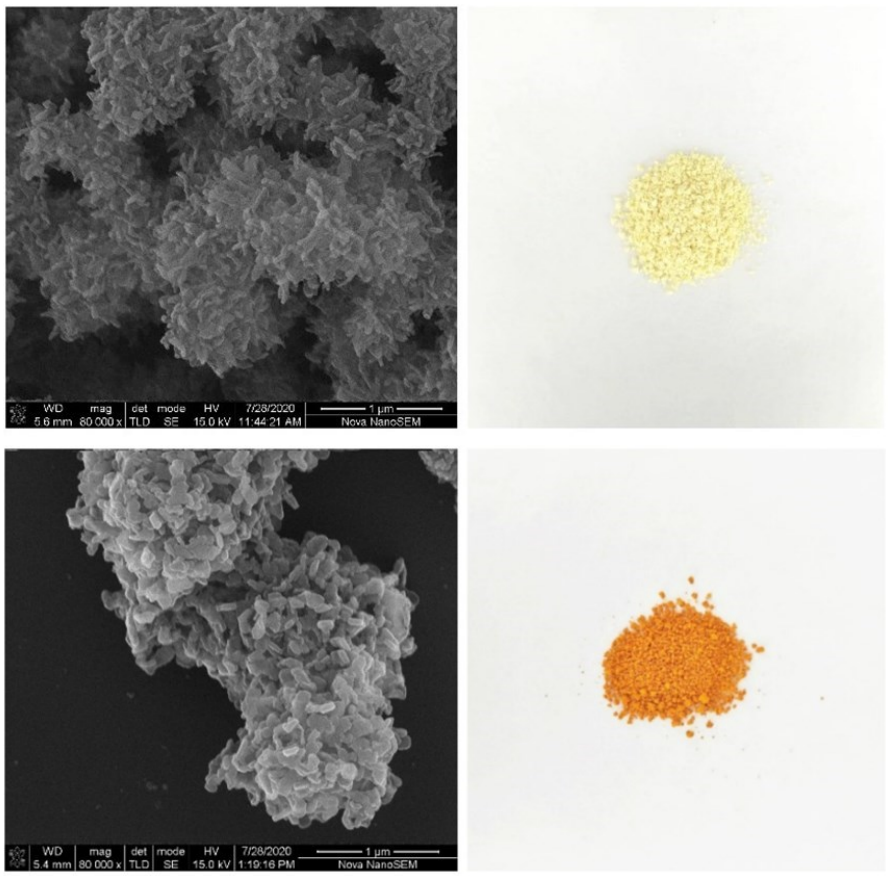


**Figure S5.** SEM images of TJNU-203 (Top) and TJNU-204 (Bottom).

## Section S5: Thermogravimetric Analysis (TGA)

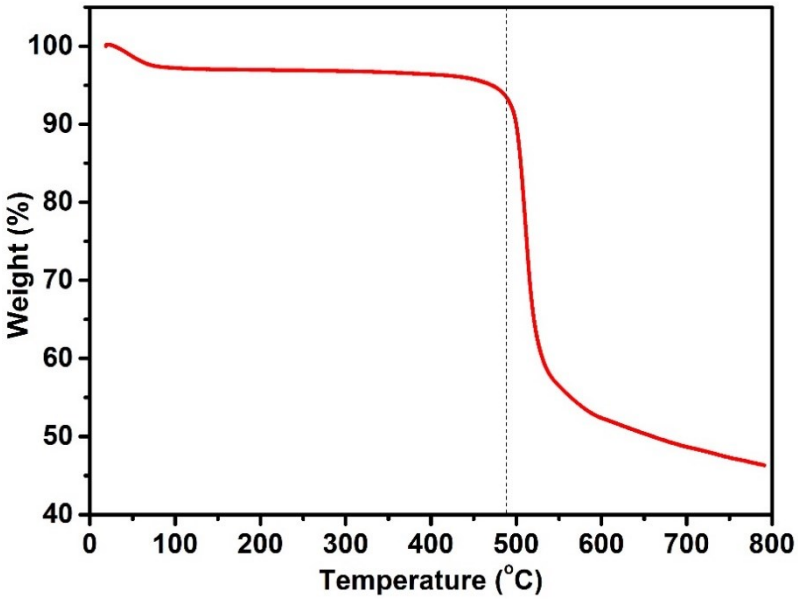


**Figure S6.** TGA curve of TJNU-203.

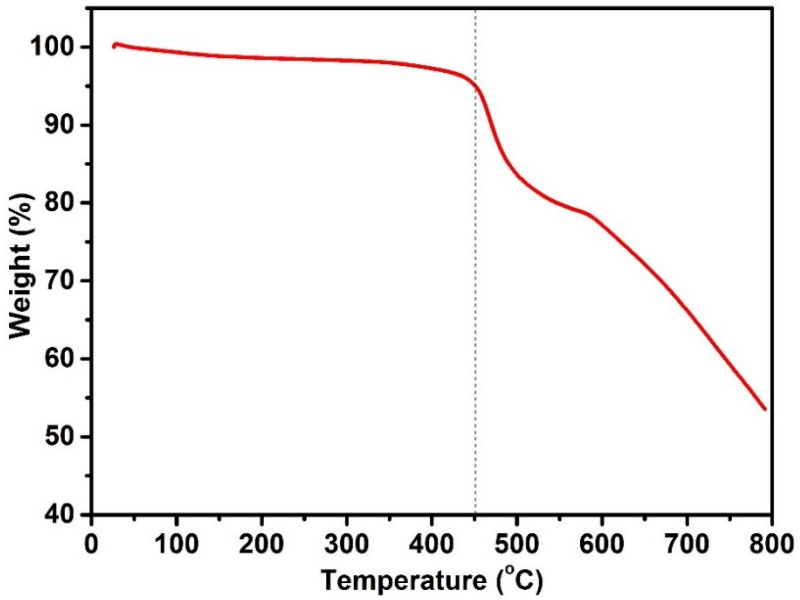


**Figure S7.** TGA curve of TJNU-204.

## Section S6: Powder X-Ray Diffraction (PXRD) Analysis

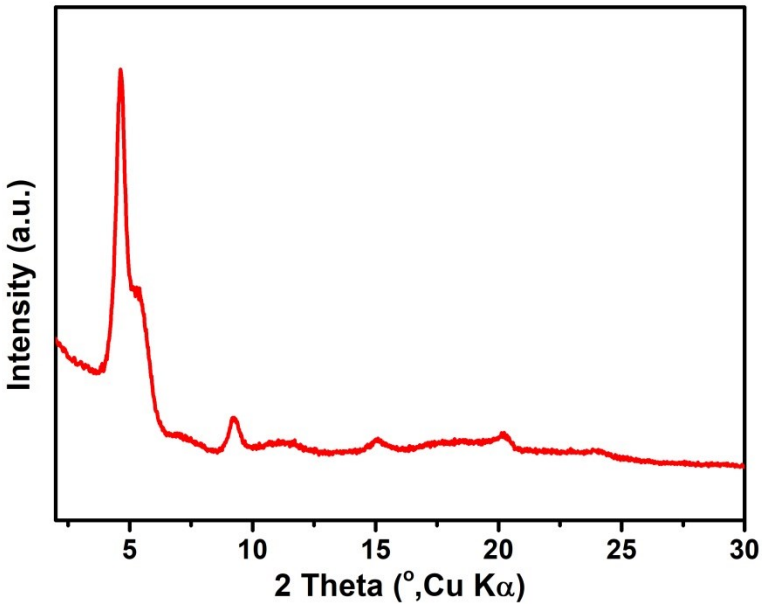


**Figure S8.** Experimental PXRD pattern of TJNU-203.

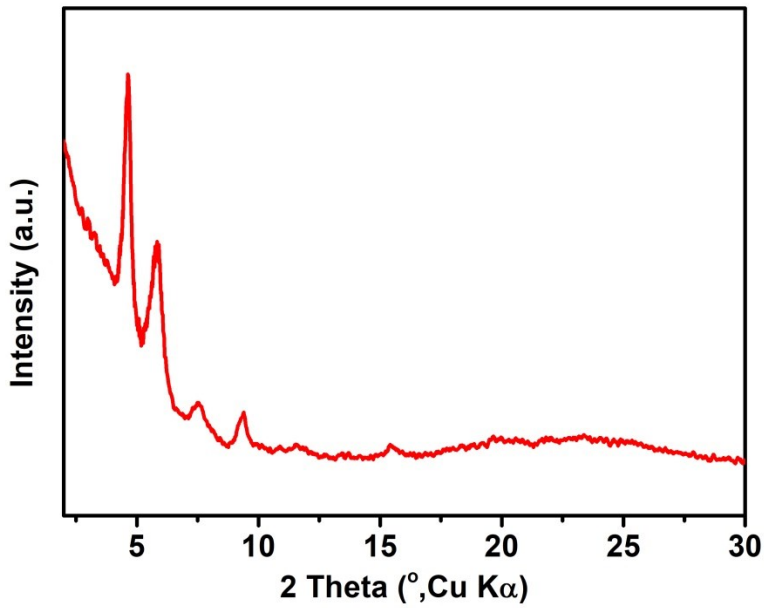


**Figure S9.** Experimental PXRD pattern of TJNU-204.

## Section S7: Structural Modeling and Crystallographic Data

The structures of TJNU-203 and TJNU-204 were determined by PXRD analysis, where the molecular modeling and Pawley refinement were carried out using Reflex, a software package implemented in MS modeling version, 4.4 (Accelrys Inc).[S5] Firstly, the lattice model was geometrically optimized using the MS Forcite molecular dynamics module. Then, we established the unit cells for TJNU-203 and TJNU-204 based on 2D structures. Both the eclipsed ($P\bar{3}m$, no 164) and staggered stacking modes (*P3m,* no 156) were considered for TJNU-203 and TJNU-204. However, all the simulated PXRD patterns did not match with the experimental patterns (Figure S11, S12, S15 and S16). Thus, the ABC stacking mode based on the space $R\bar{3}m$ (no. 166) was constructed for TJNU-203 and TJNU-204, affording the unit cell parameters of $a = b = 38.127$ Å and $c = 17.300$ Å for TJNU-203 and $a = b = 38.012$ Å and $c = 19.030$ Å for TJNU-204. The simulated PXRD patterns are in good agreement with the experimental patterns in terms of both peak positions and relative intensities (Figure S13 and S17). Finally, Pawley refinement was performed to optimize the lattice parameters iteratively until the RWP value converged (Figure 2), yielding good agreement factors (wRp = 4.07%, Rp = 3.27% for TJNU-203 and wRp = 4.06%, Rp = 2.83% for TJNU-204).

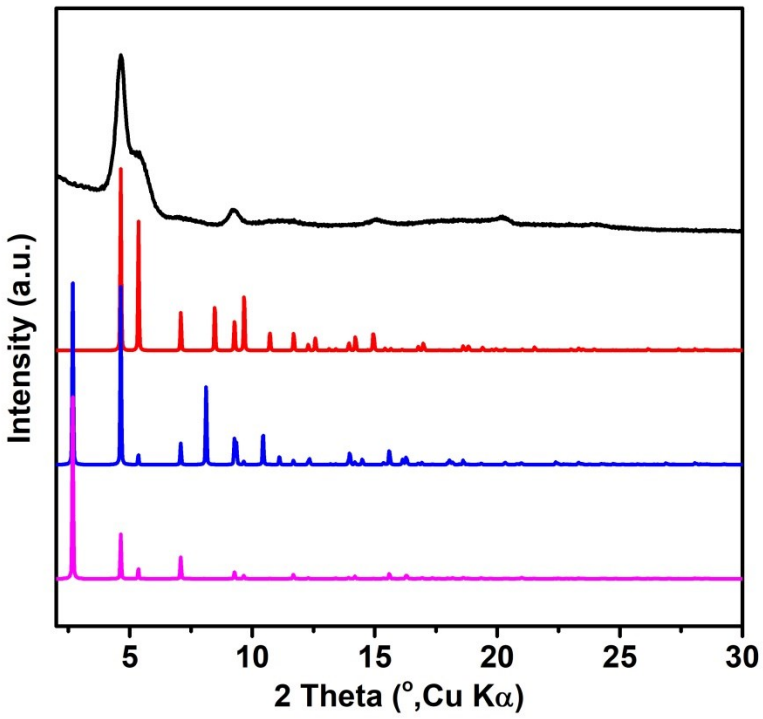


**Figure S10.** Experimental PXRD pattern (black), the simulated ABC (red), staggered AB (blue) and eclipsed AA (purple) stacking patterns of TJNU-203.

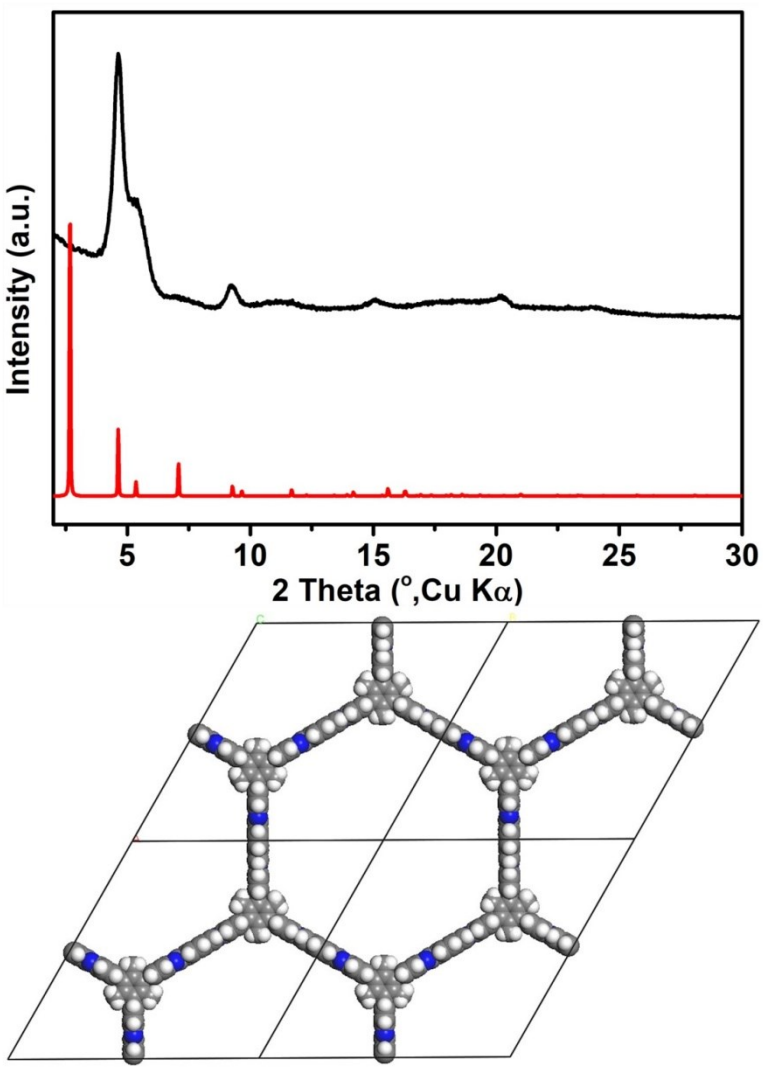


**Figure S11.** Experimental PXRD pattern (black) and the simulated eclipsed AA stacking pattern (red) of TJNU-203 (Top). Unit cell of eclipsed AA stacking mode for TJNU-203 (Bottom).

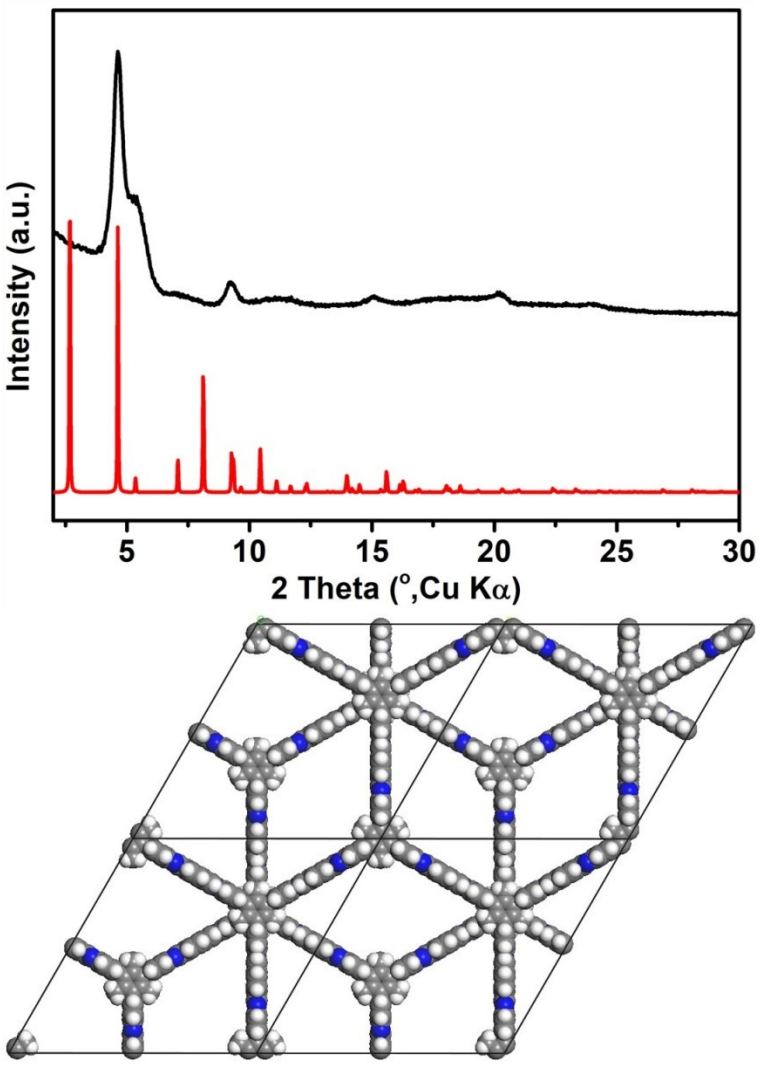


**Figure S12.** Experimental PXRD pattern (black) and the simulated staggered AB stacking pattern (red) of TJNU-203 (Top). Unit cell of staggered AB stacking mode for TJNU-203 (Bottom).

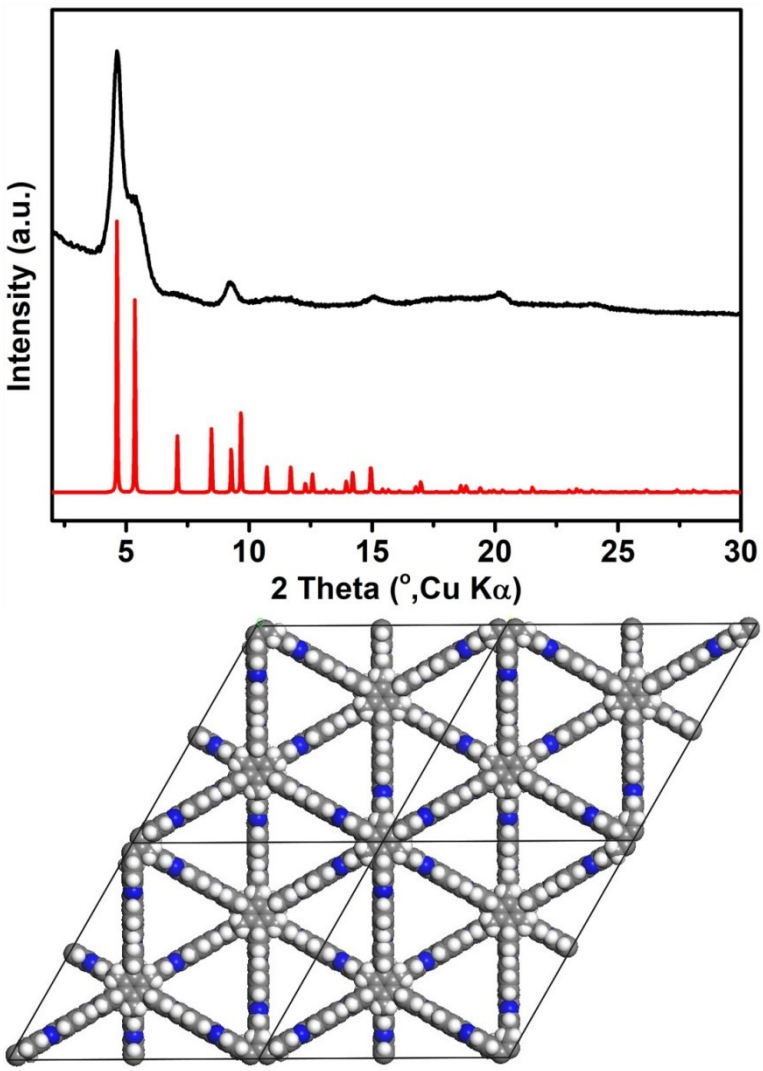


**Figure S13.** Experimental PXRD pattern (black) and the simulated ABC stacking pattern (red) of TJNU-203 (Top). Unit cell of ABC stacking mode for TJNU-203 (Bottom).

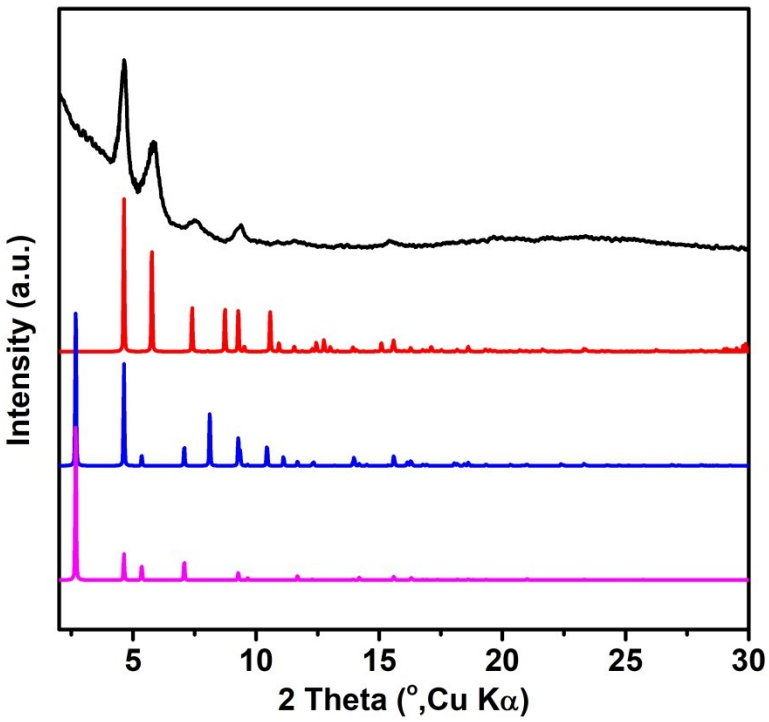


**Figure S14.** Experimental PXRD pattern (black), the simulated ABC (red), staggered AB (blue) and eclipsed AA (purple) stacking patterns of TJNU-204.

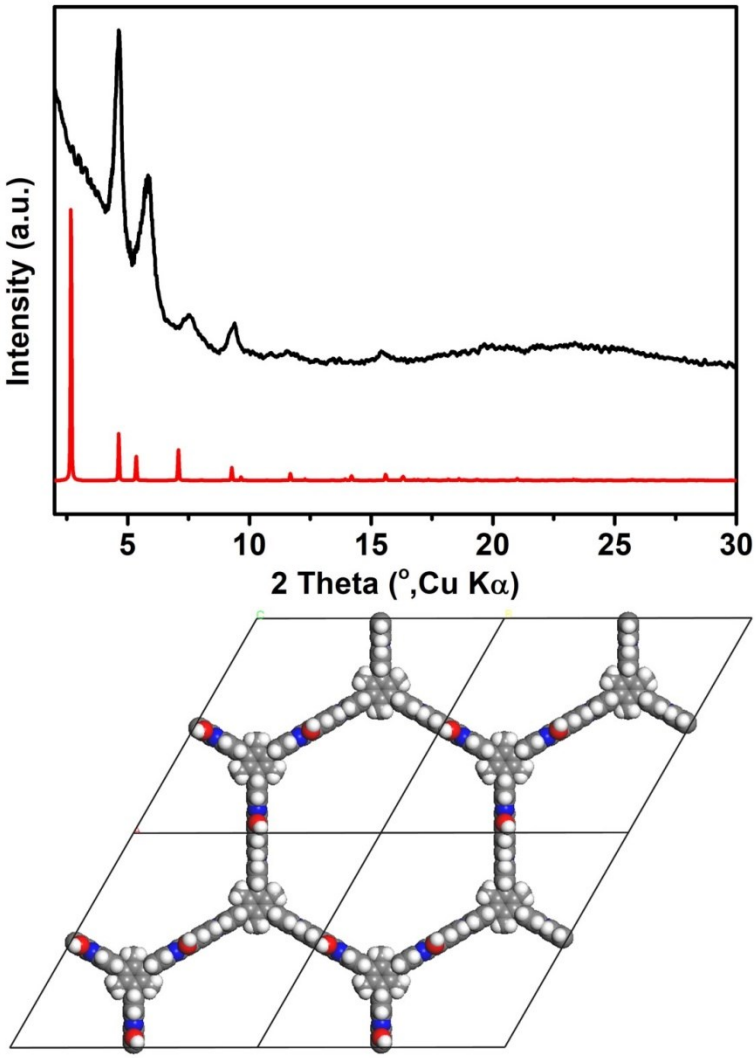


**Figure S15.** Experimental PXRD pattern (black) and the simulated eclipsed AA stacking pattern (red) of TJNU-204 (Top). Unit cell of eclipsed AA stacking mode for TJNU-204 (Bottom).

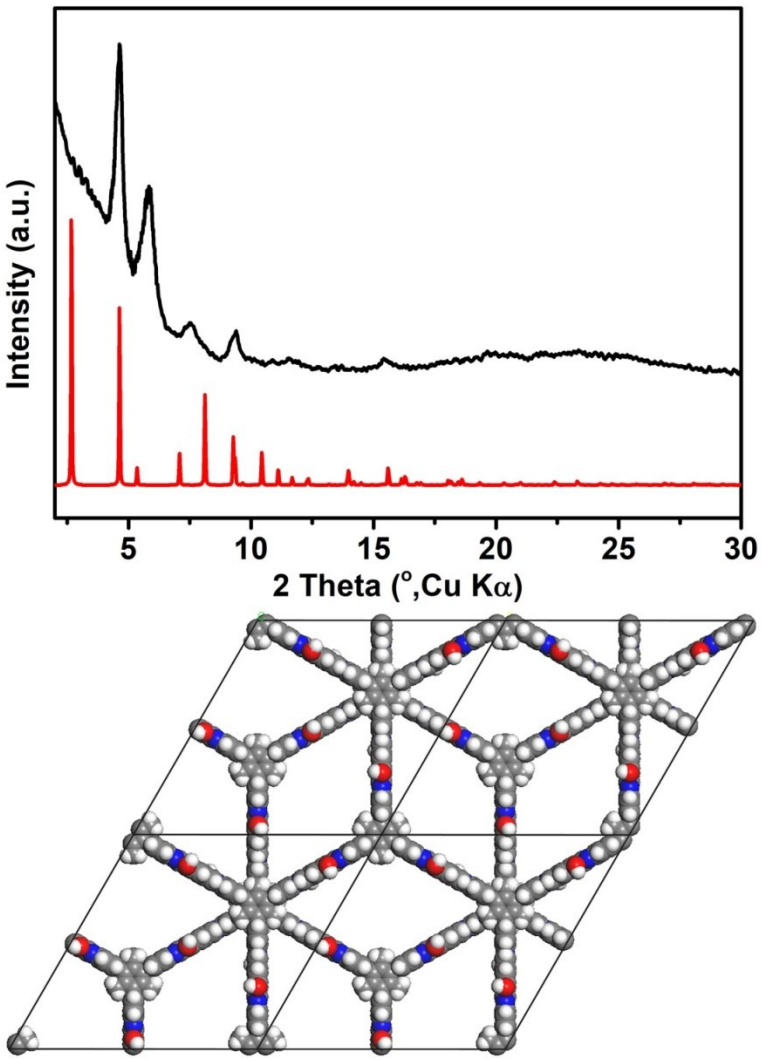


**Figure S16.** Experimental PXRD pattern (black) and the simulated staggered AB stacking pattern (red) of TJNU-204 (Top). Unit cell of staggered AB stacking mode for TJNU-204 (Bottom).

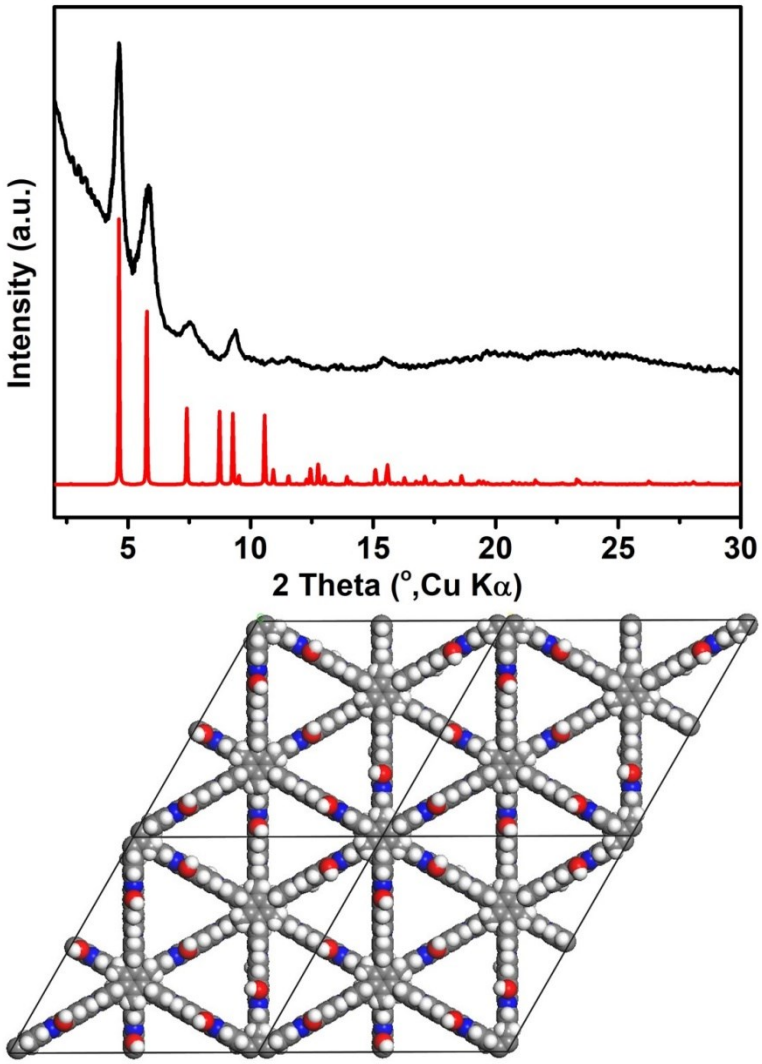


**Figure S17.** Experimental PXRD pattern (black) and the simulated ABC stacking pattern (red) of TJNU-204 (Top). Unit cell of ABC stacking mode for TJNU-204 (Bottom).

**Table S1.** Fractional atomic coordinates for the unit cell of TJNU-203 calculated from the Materials Studio Modeling program.

| TJNU-203 space group: $R\bar{3}m$<br>$a = b = 38.1257$ Å; $c = 19.0294$ Å<br>$\alpha = \beta = 90°$; $\gamma = 120°$ | | | | |
|---|---|---|---|---|
| C1 | C | 0.48893 | 0.51114 | 0.06678 |
| C2 | C | 0.47783 | 0.52224 | -0.00004 |
| C3 | C | 0.45560 | 0.54447 | -0.00008 |
| N4 | N | 0.44450 | 0.55557 | -0.06690 |
| C5 | C | 0.42227 | 0.57780 | -0.06695 |
| C6 | C | 0.41115 | 0.58892 | -0.00017 |
| C7 | C | 0.38892 | 0.61115 | -0.00022 |
| C8 | C | 0.37782 | 0.62225 | -0.06704 |
| C9 | C | 0.38894 | 0.61112 | -0.13381 |
| C10 | C | 0.41117 | 0.58890 | -0.13377 |
| C11 | C | 0.35559 | 0.64448 | -0.06708 |
| C12 | C | 0.37779 | 0.68893 | -0.06708 |
| C13 | C | 0.42225 | 0.71118 | -0.06708 |
| C14 | C | 0.82229 | 0.64452 | 0.59988 |

**Table S2.** Fractional atomic coordinates for the unit cell of TJNU-204 calculated from the Materials Studio Modeling program.

| TJNU-204 space group: $R\bar{3}m$<br>$a = b = 38.0124$ Å; $c = 17.3007$ Å<br>$\alpha = \beta = 90°$; $\gamma = 120°$ | | | | |
|---|---|---|---|---|
| C1 | C | 0.48892 | 0.51112 | 0.07346 |
| C2 | C | 0.47782 | 0.52223 | -0.00004 |
| C3 | C | 0.48894 | 0.51110 | -0.07349 |
| C4 | C | 0.45559 | 0.54445 | -0.00009 |
| N5 | N | 0.44449 | 0.55556 | -0.07359 |
| C6 | C | 0.42226 | 0.57778 | -0.07364 |
| C7 | C | 0.41114 | 0.58891 | -0.00019 |
| C8 | C | 0.38891 | 0.61113 | -0.00024 |
| C9 | C | 0.37781 | 0.62224 | -0.07373 |
| C10 | C | 0.38893 | 0.61111 | -0.14718 |
| C11 | C | 0.41116 | 0.58888 | -0.14713 |
| O12 | O | 0.47786 | 0.52219 | -0.14687 |
| C13 | C | 0.35558 | 0.64446 | -0.07378 |
| C14 | C | 0.37779 | 0.68892 | -0.07378 |
| C15 | C | 0.42224 | 0.71116 | -0.07378 |

## Section S8: Porosity and Specific Surface Area Analysis

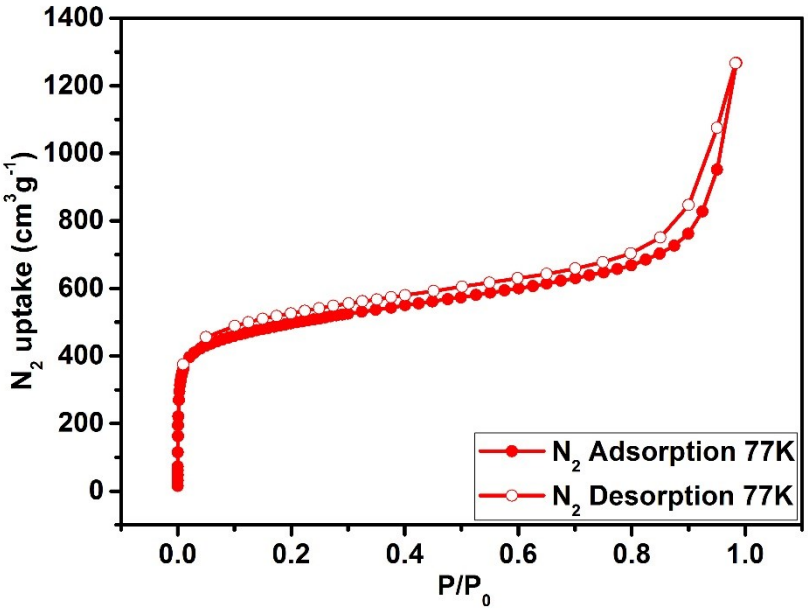


**Figure S18.** $N_2$ adsorption/desorption isotherms of TJNU-203 at 77 K.

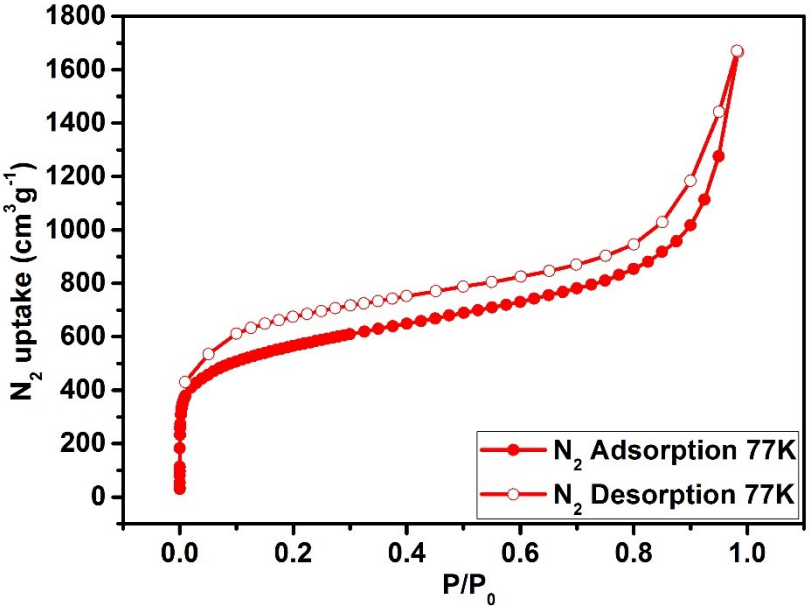


**Figure S19.** $N_2$ adsorption/desorption isotherms of TJNU-204 at 77 K.

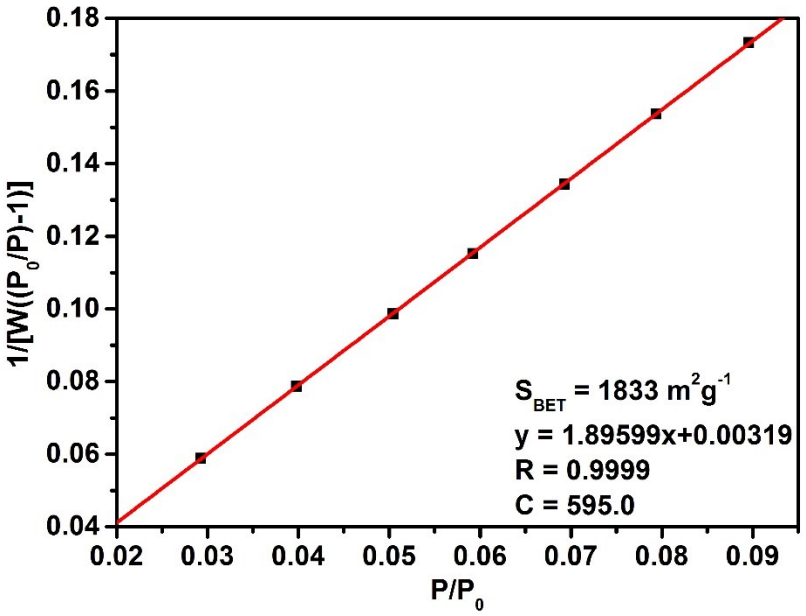


**Figure S20.** BET plot of TJNU-203 calculated from $N_2$ adsorption isotherm at 77 K, with C value of 595.0.

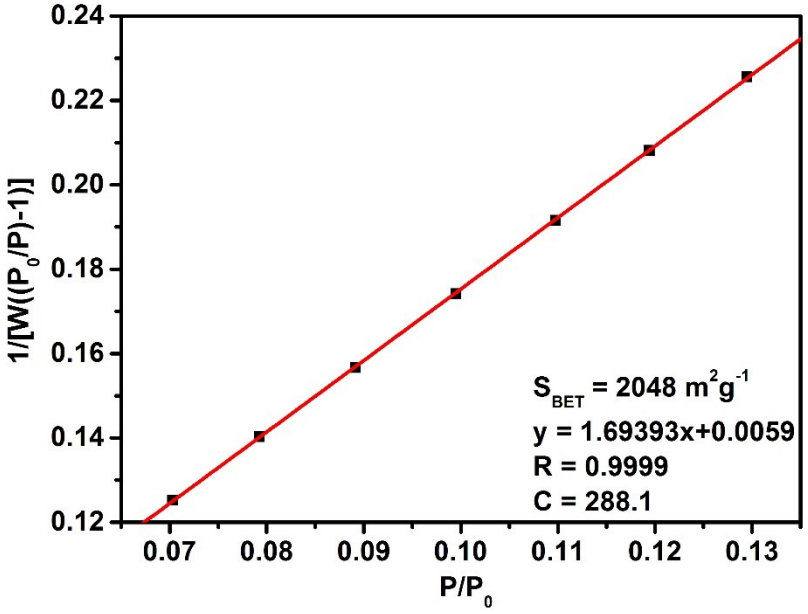


**Figure S21.** BET plot of TJNU-204 calculated from $N_2$ adsorption isotherm at 77 K, with C value of 288.1.

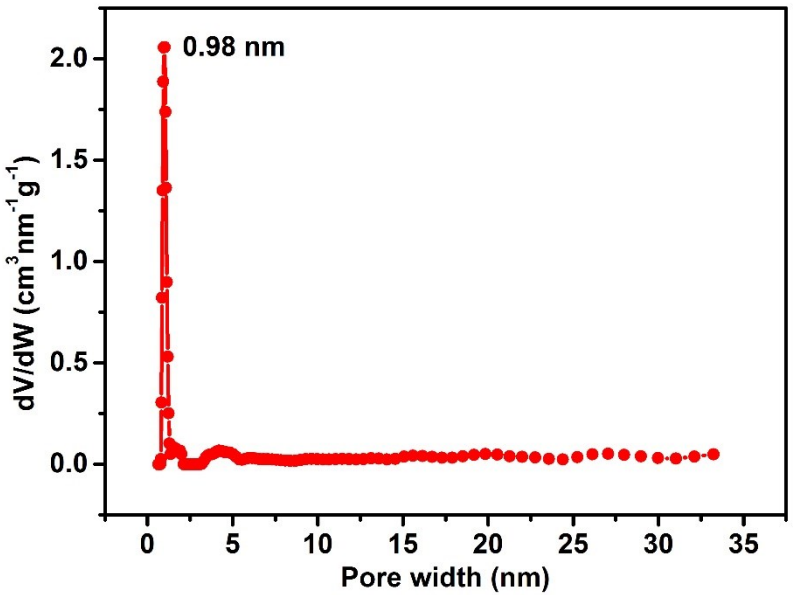


**Figure S22.** Pore size distribution of TJNU-203.

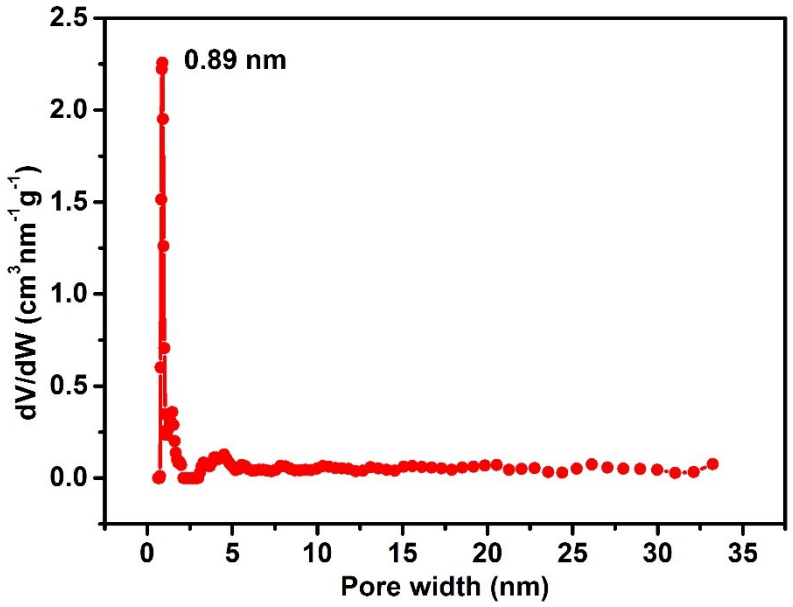


**Figure S23.** Pore size distribution of TJNU-204.

## Section S9: Iodine Capture Experiments

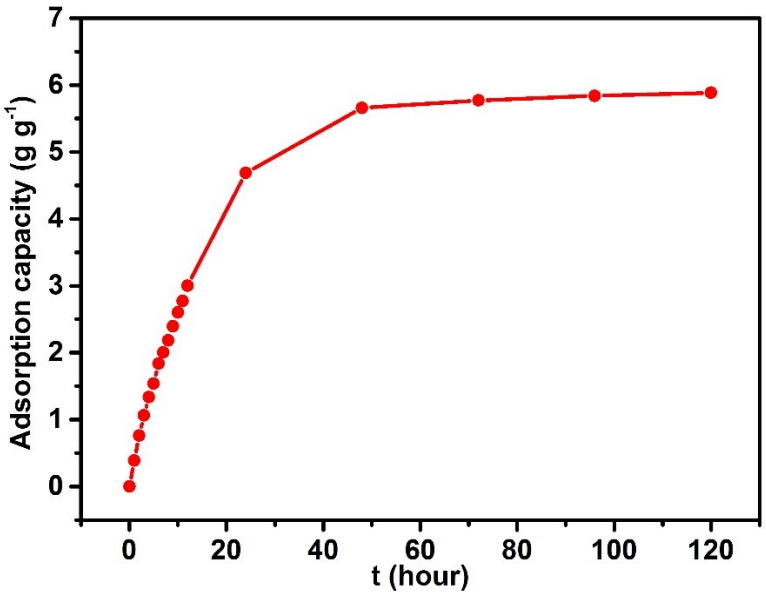


**Figure S24.** Gravimetric uptake of $I_2$ vapor by TJNU-203 as a function of time at 77 ºC and ambient pressure.

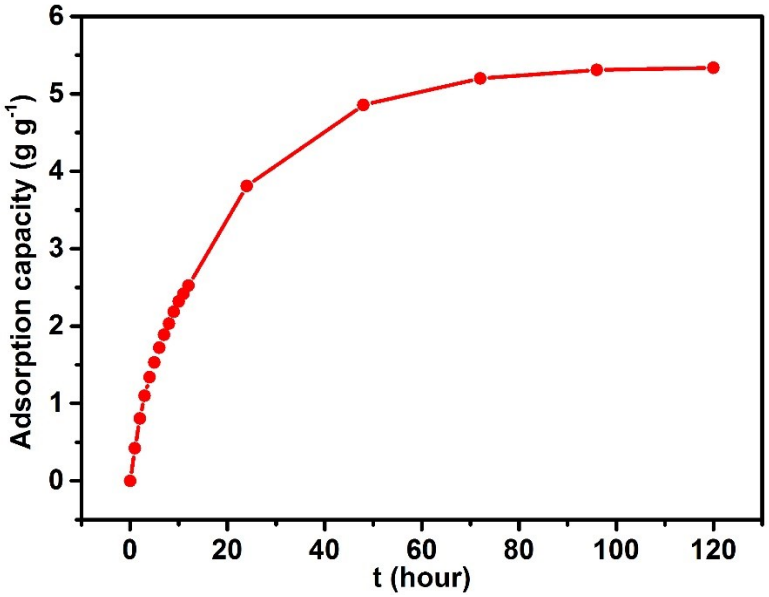


**Figure S25.** Gravimetric uptake of $I_2$ vapor by TJNU-204 as a function of time at 77 ºC and ambient pressure.

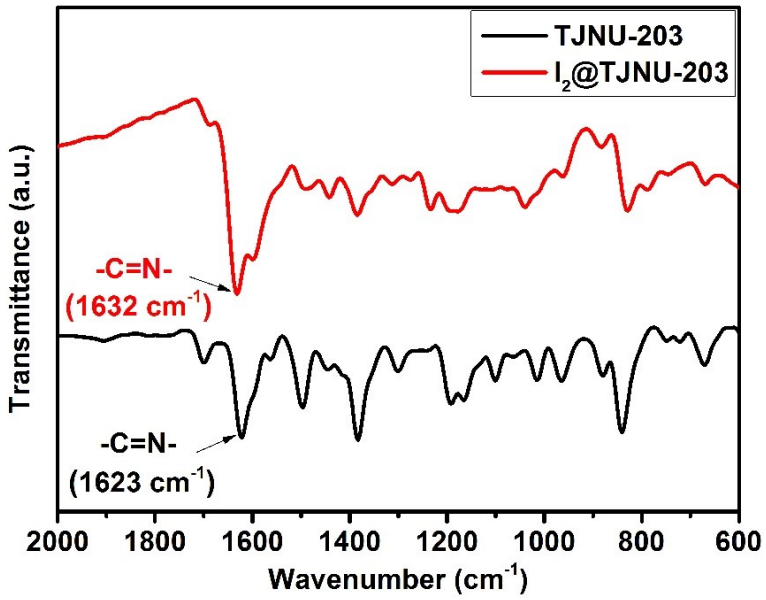


**Figure S26.** FT-IR spectra of TJNU-203 (black line) and $I_2$@TJNU-203 (red line).

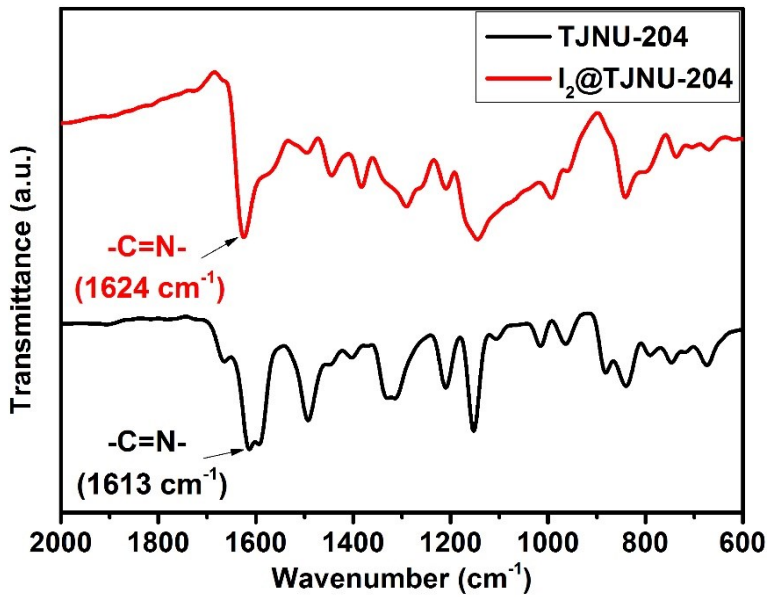


**Figure S27.** FT-IR spectra of TJNU-204 (black line) and $I_2$@TJNU-204 (red line).

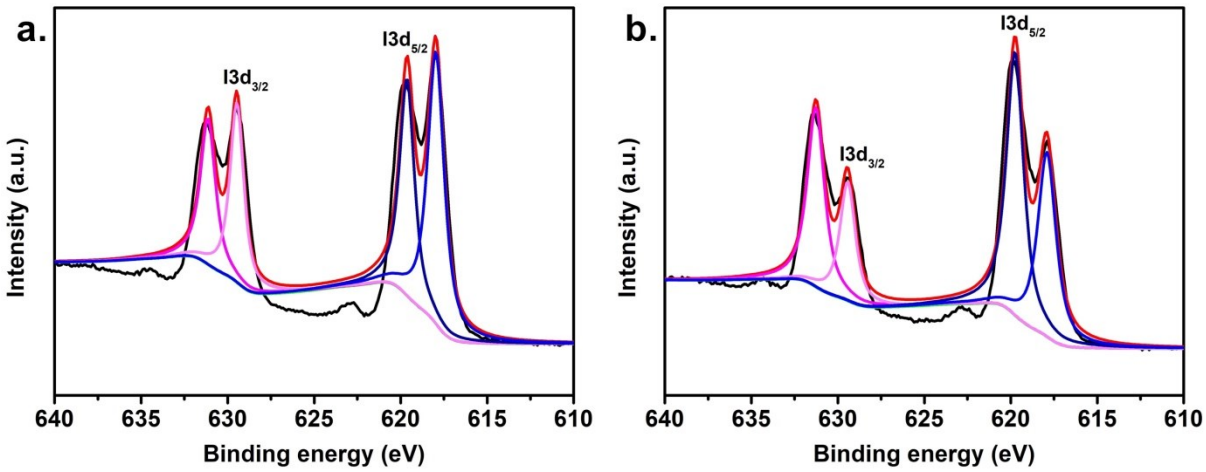


**Figure S28**. XPS spectra of $I3d_{3/2}$ and $I3d_{5/2}$ for (a) TJNU-203 and (b) TJNU-204 after iodine adsorption.

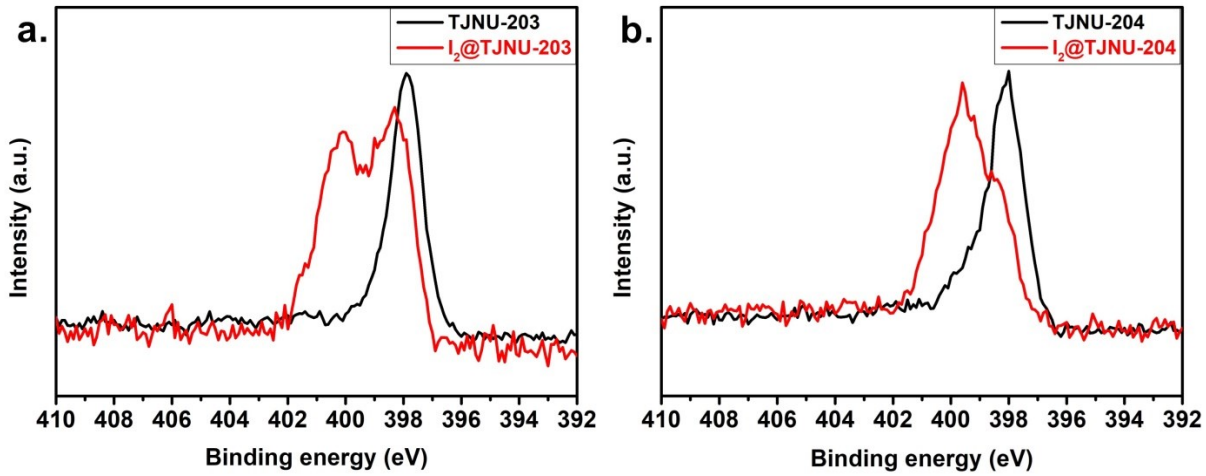


**Figure S29**. XPS spectra of N1s for (a) TJNU-203 and (b) TJNU-204 before and after iodine adsorption.

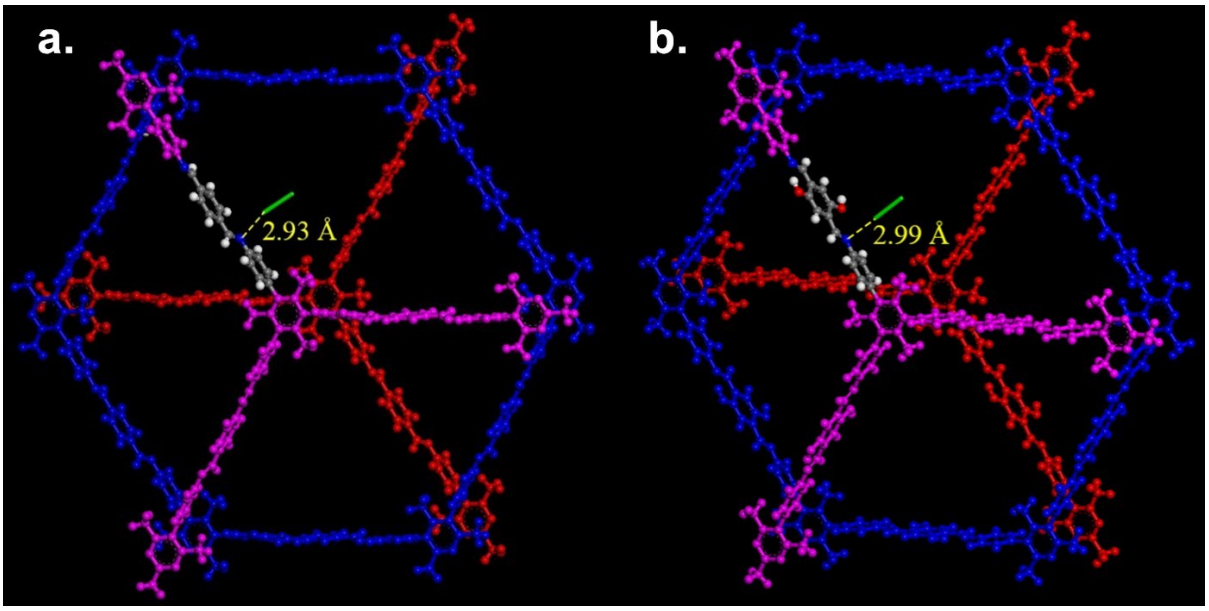


**Figure S30**. Optimized configurations of (a) $I_2$@TJNU-203 and (b) $I_2$@TJNU-204 ($I_2$: green).

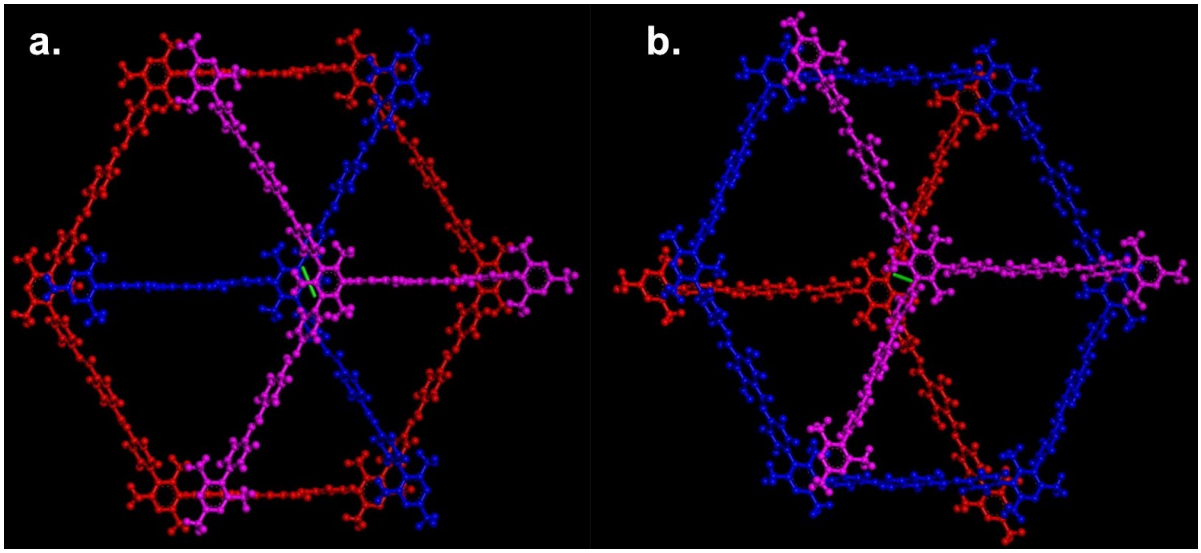


**Figure S31**. $I_2$ located in the space between the two aromatic rings in (a) TJNU-203 and (b) TJNU-204 ($I_2$: green).

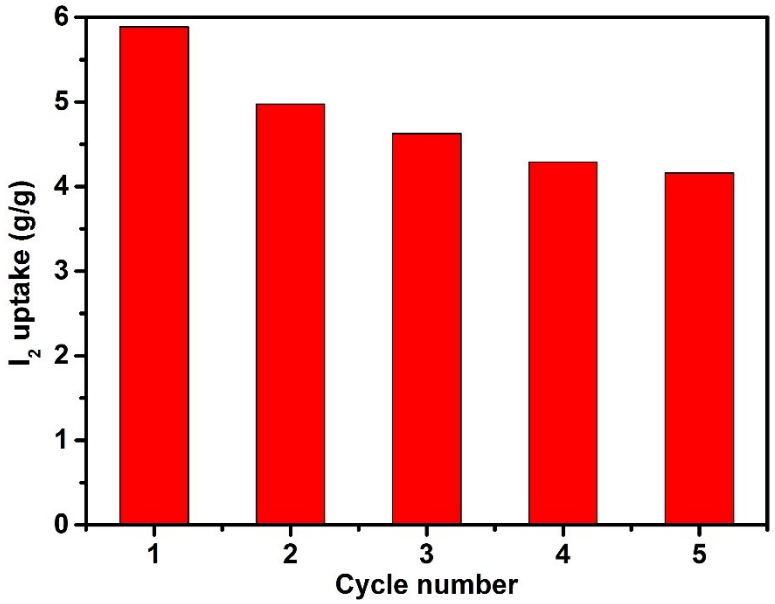


**Figure S32.** Iodine vapor capture cycle of TJNU-203.

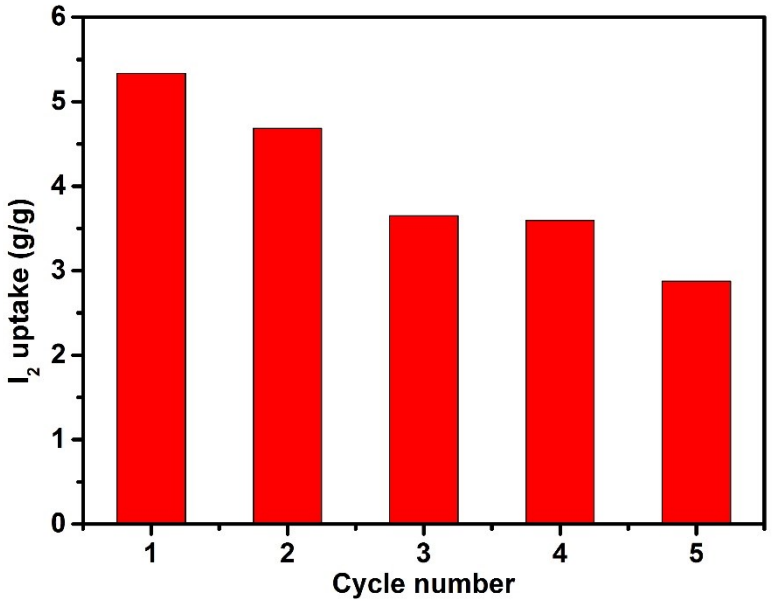


**Figure S33.** Iodine vapor capture cycle of TJNU-204.

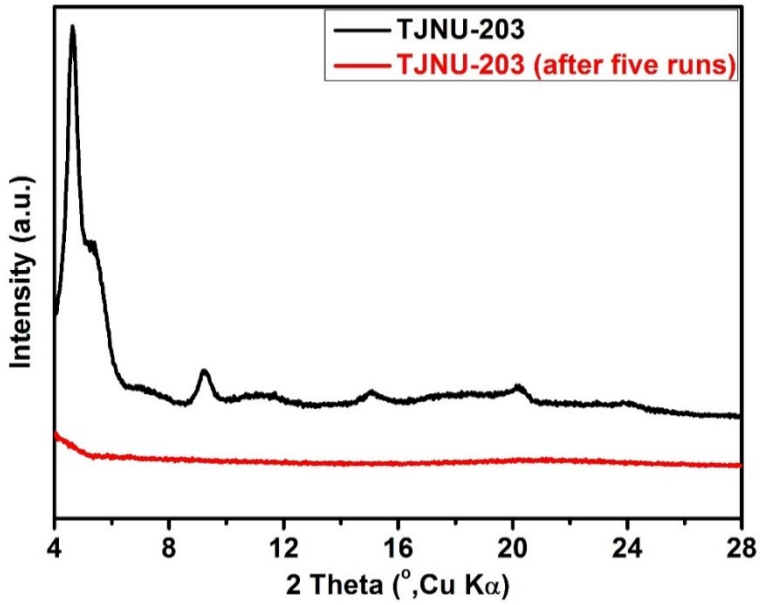


**Figure S34.** PXRD patterns of TJNU-203 (black line) and recycled TJNU-203 after five runs of iodine vapor capture and release (red line).

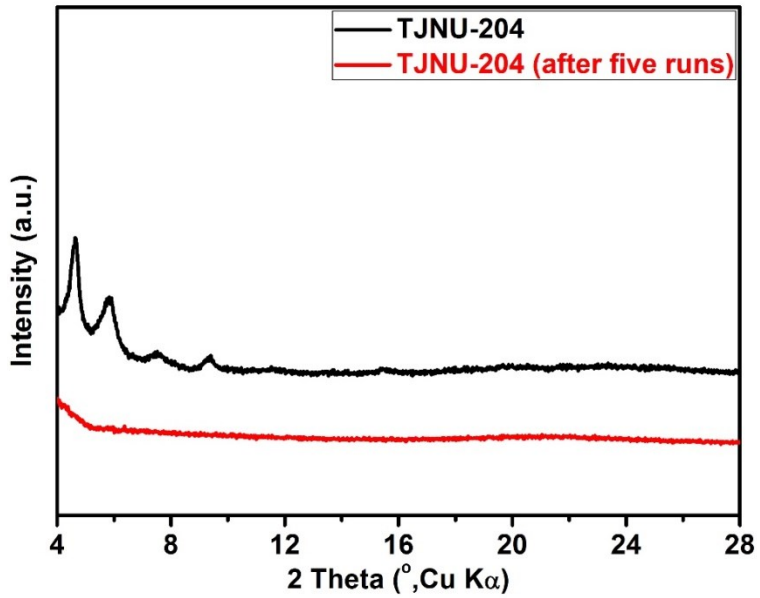


**Figure S35.** PXRD pattern of TJNU-204 (black line) and recycled TJNU-204 after five runs of iodine vapor capture and release (red line).

## Section S10: References

S1. J. Li, H. Zhang, L. Zhang, K. Wang, Z. Wang, G. Liu, Y. Zhao and Y. Zeng, *J. Mater. Chem. A.,* 2020, **8**, 9523-9527.

S2. Y. Zeng, X. Zhu, Y. Yuan, X. Zhang and S. Ju, *Sep. Purif. Technol.*, 2012, **95**, 149-156.

S3. B. Supronowicz, A. Mavrandonakis and T. Heine, *J. Phys. Chem. C*, 2013, **117**, 14570-14578.

S4. L. Hamon, H. Leclerc, A. Ghoufi, L. Oliviero, A. Travert, J.-C. Lavalley, T. Devic, C. Serre, G. Férey, G. De Weireld, A. Vimont and G. Maurin, *J. Phys. Chem. C*, 2011, **115**, 2047-2056.

S5. Accelrys, Material Studio Release Notes, Release 4.4, Accelrys Software, San Diego 2008.